# Hydrogen Bonding at the Aerosol Interface

**Jian-Xiang Zhang, Denise Aiello, and Pamela M. Aker***

*Department of Chemistry, University of Pittsburgh, Pittsburgh, Pennsylvania 15260*

*Received: March 24, 1994; In Final Form: September 13, 1994*[⊗]

Morphology-dependent stimulated Raman scattering (MDSRS) has been used to monitor the degree of hydrogen bonding in water aerosols generated by a vibrating orifice aerosol generator (VOAG). The results show that aerosols created by a VOAG suffer extensive structural disruption and that the disruption is most pronounced at the aerosol surface. Laboratory aerosols prepared in this way do not appropriately mimic those found in the atmosphere, and the mass accommodation coefficients measured using such aerosols should not be used in global climate modeling calculations.

## Introduction

It is well established that heterogeneous interactions play an important role in determining the chemistry of the troposphere and stratosphere. Global climate models (GCM), which are used to predict the impact of anthropogenic emissions on the earth's atmosphere, have now been modified to include these reactions. Recent studies show that GCM output is quite sensitive to the heterogeneous rates.[1] A precise prediction of future atmospheric change can therefore be achieved only if the rates used in the calculation accurately reflect those found naturally. The surfaces found in the natural atmosphere are at equilibrium, for aerosol lifetimes are on the order of days to weeks, hence laboratory experiments must use surfaces which fit this description.

In recent years, a considerable amount of effort has been focused on measuring mass accommodation coefficients on liquid aerosol surfaces.[2] A variety of surface generation methodologies have been used. The most popular appears to be the vibrating orifice aerosol generator (VOAG), principally because the apparatus is simple, inexpensive, and easily incorporated into a machine designed for kinetics studies. However, we show here that caution must be exercised when using such an apparatus in a heterogeneous kinetics experiment, for the VOAG produces aerosols which are not at equilibrium, at least for the first 5 ms of their life. In specific, the nascent aerosols, and their surfaces, are severely hydrogen bond disrupted.

We have used a novel nonlinear Raman spectroscopic technique to monitor the chemical composition, and molecular structure, of aerosols created by a VOAG. The technique is morphology-dependent stimulated Raman scattering (MDSRS). Although the phenomenology of MDSRS, and its application for determining the chemical properties of aerosols, has been the subject of a number of research investigations,[3−6] the technique, to say the least, is not well-known in the general scientific community. We will therefore outline some pertinent details associated with MDSRS spectroscopy before we describe our experimental results. For details beyond what is presented in this paper the reader is referred to the bibliographic compendium contained in ref 6. In addition, we also briefly outline the interpretation of the liquid water Raman spectrum in the O−H stretch region, for an understanding of this is needed to interpret the degree of hydrogen bond disruption observed in aerosols generated by using a vibrating orifice.

## Morphology-Dependent Stimulated Raman Scattering (MDSRS)

It is well-known that all particles with regular structure, i.e., spheres, cubes, ellipsoids, cylinders, etc., have a set of virtual (cavity) modes.[7−10] These virtual modes are called morphology-dependent resonances (MDRs) because their existence is determined by particle size, shape, and refractive index. MDRs participate in optical absorption and scattering phenomena; their participation is evidenced by an enhancement in the optical transition moment of the material being probed. The enhancement arises because the cavity resonances contribute to the density of states underneath a material's optical transition. A representative example of an MDR enhanced optical system is the laser. MDSRS is simply stimulated Raman scattering performed in an optical cavity. Aerosols are optical cavities, albeit small in size. Hence it is trivial to generate stimulated Raman scattering in aerosols.

The theory associated with small particle cavity resonances is well developed.[7−10] Studies show that the MDRs associated with spheroids and ellipsoids are physically located at the rim of the particle. The depth of penetration of an MDR into the bulk structure is dictated by its radial and angular mode numbers, denoted as $n$ and $l$. As van de Hulst has shown, the location of the internal intensity maximum of a particular mode is given by[10]

$$r_{MDR} \sim (n + 1/2)\lambda_{MDR}/2\pi m \qquad (1)$$

where $m$ is the refractive index of the material comprising the cavity. Most of the intensity is distributed over an area, $\pi\Delta r_{MDR}^2$, where

$$\Delta r_{MDR} = n\Delta\lambda_{MDR}/2\pi m = n\lambda_{MDR}/2\pi m Q_{MDR} \qquad (2)$$

and $Q_{MDR} = \lambda_{MDR}/\Delta\lambda_{MDR}$.[6b] (The $Q$ value of an MDR is a measure of the amount of energy which can be stored in the mode.) Equation 2 is valid only for low-$Q$ modes ($Q < 10^5$), for diffraction limits the volume over which this intensity is distributed to a value greater than $(\lambda/2)^3$. The mode volume is given by $\pi\Delta r_{MDR}^2 \times 2\pi r_{MDR} = \pi\Delta r_{MDR}^2 \times n\lambda_{MDR}/m$. Thus in the diffraction limit, which is the case in our experiments,

$$\Delta r_{MDR} \sim [m\lambda^2/8\pi n]^{1/2} \qquad (3)$$

MDSRS is generated in aerosols when an incident green (pump) light source is brought close to the equatorial edge of

[⊗] Abstract published in *Advance ACS Abstracts*, December 15, 1994.

0022-3654/95/2099-0721$09.00/0 

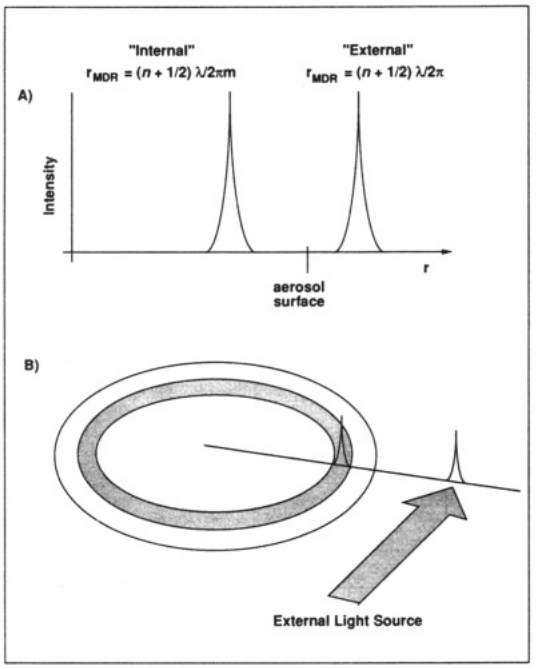


**Figure 1.** (A) Internal and external intensity distributions of an arbitrary cavity mode. (B) Excitation of an internal cavity mode by an external light source.

an aerosol. Green (pump) light can be coupled into the aerosol, in spite of the fact that the light is not directly incident on the aerosol body, because MDRs have intensity maxima located both internal and external to the aerosol body.[7b,9] This intriguing physics stems from the fact that there are degenerate solutions to the Hankel and Bessel functions which describe the MDR spectral and spatial location. The degeneracy arises because the equations can be solved for the case where the refractive index of the cavity is that associated with the material comprising the aerosol or for the case where the refractive index of the cavity is that of air (or the medium surround the aerosol). In air, the external mode's intensity maximum occurs at $r_{MDR} = n\lambda_{MDR}/2\pi$, since $m = 1$. Figure 1A depicts the internal and external MDR intensity distributions for an arbitrary mode. Figure 1B illustrates how light intensity external to the cavity is coupled into the interior; i.e., excitation of the external mode by a foreign light source simultaneously induces excitation in the internal mode. Once the light has been coupled into a cavity mode, it remains trapped for the lifetime, $\gamma$, of the mode, or until it is annihilated by some optical process. The net effect of this trapping is to increase the sample path length to $1 = c\gamma/m$.

MDSRS occurs when there is a coupling between a green (pump) MDR and a red (Stokes) MDR. Modes couple when they have identical $L_z$ ($= |L| \cos \phi = n_m$, where $\phi$ is the azimuthal angle, $n_m$ is the azimuthal mode number, and $L^2 = n(n+1)$),[6b] i.e. identical $n_m$. The red mode provides a localized electric field oscillating at $\omega_s$. The local field changes the polarization and therefore enhances the Raman scattering cross section by a factor which is determined by the mode's electric field, which at $r_{MDR}$ is directly proportional to the red mode $Q$. Note that only those molecules in the red mode volume experience the enhanced field; thus, the net Raman scattering enhancement seen is determined by the degree of radial, $\phi_r$, angular, $\phi_\theta$, and azimuthal, $\phi_\phi$, overlap between the red mode and the green mode volumes. This is shown in Figure 2.

Once the light in the green mode has been Raman shifted, it can either scatter from the aerosol (i.e. red light does not stay trapped in a green mode) or become trapped in the red mode

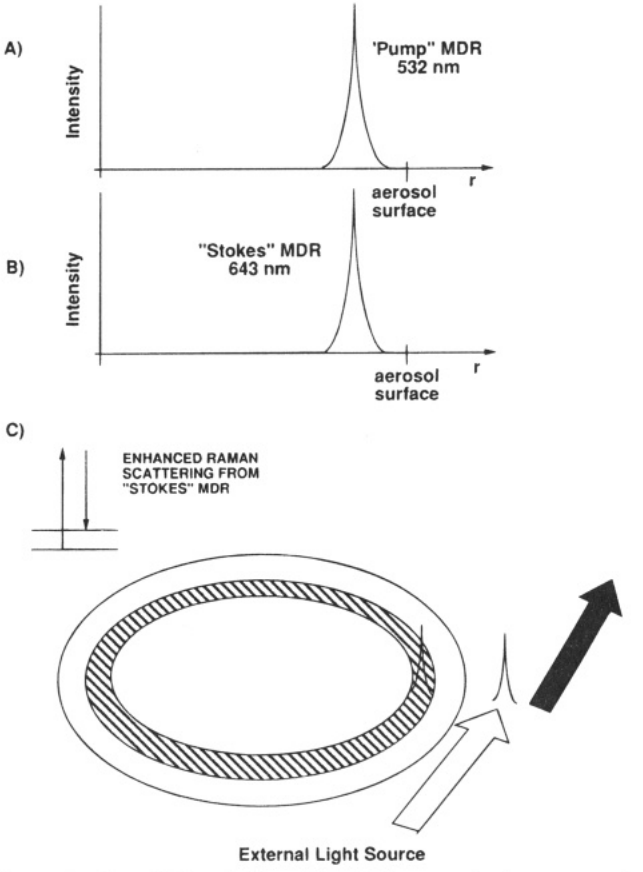


**Figure 2.** Pictorial description of MDSRS generation in an aerosol. (A) Internal intensity distribution of a "pump" mode. (B) Internal intensity distribution of a "Stokes" mode. (C) Excitation of a "Stokes" mode via Raman scattering.

volume. The Raman-shifted light that is scattered from the green mode maintains the green mode angular characteristics, but is phase shifted.[6b] The phase shift causes the red light to appear as arising from a point source at $r_{ext} = (n_{green} + 1/2)\lambda_{red}/2\pi$, which is further from the sphere origin than the green point source which appears to occur at $r_{ext} = (n_{green} + 1/2)\lambda_{green}/2\pi$. A pictorial description of this interesting effect is shown in Figure 2C, and photographic confirmation can be found in ref 3.

The position of the intensity maximum of the foreign light source, with respect to the cavity center, determines the identity of the green (and therefore red) cavity mode excited during the illumination process. MDRs with identical $l$ but increasing $n$ have approximately equal $Q$ values ($Q$ typically increases by only 1−3% with $\Delta n = 1$), but as eq 1 shows, their external and internal intensity maxima are located at successively larger distances from the cavity center. If the excitation beam is brought in at successively larger distances away from the cavity center, then modes with successively larger $n$, and therefore successively larger $r$, will be excited. This is shown in Figure 3. MDSRS can therefore be used to spatially image the structural and compositional changes that occur upon traversal from the bulk through the interface. This imaging capability is most unusual and is extremely opportunistic, especially with regard to liquid interfaces, for MDSRS can be used to obtain molecular pictures of a region which has, up until now, proved elusive to experimental probing.

The actual gain realized in an MDSRS experiment is typically smaller than that predicted theoretically. This arises because other optical processes, such as absorption and Rayleigh scattering, will compete with Raman scattering to reduce the

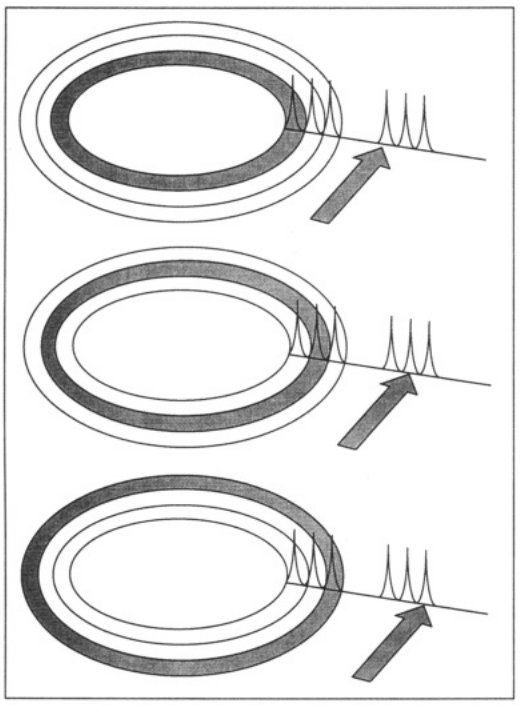

**Figure 3.** Translation of the incident laser beam away from the aerosol surface allows cavity modes with larger radii to be excited. This illumination scheme can be used to spatially image structural changes that occur in the liquid−air interface.

intensity of the green (pump) light in the cavity. In addition, MDR $Q$ values can be degraded by temporal or spatial gradients in the optical cavity materials's refractive index. It is well-known that the refractive index is a sensitive function of temperature and pressure. The method used to prepare the sample which is to be interrogated by MDSRS is therefore extremely important. Research in our laboratory has been focused on improving MDSRS detection sensitivity in water-based aerosols representative of those found in the atmosphere. And it has, in fact, been our frustrating inability to generate MDSRS in samples which in principle should generate huge signals that led us to perform the series of experiments outlined here. Information on the molecular structure of aqueous aerosols is contained in the water MDSRS spectrum. A detailed scrutiny of the changes seen in water MDSRS signals has enabled us to show that a transient structural perturbation is present in aerosols generated by a vibrating orifice. The perturbation is the root cause of the limitation in MDSRS sensitivity.

## Interpretation of the Water Raman Spectrum

The interpretation of the liquid water Raman spectrum in the OH stretch region has a long history. As Figure 4 shows, the band spans a huge Raman shift, from ~3000 to 3600 $cm^{-1}$, has a complex structure, and, although not shown by Figure 3, has a polarization pattern that is highly temperature dependent. Efforts to unravel the meaning of the liquid Raman spectrum, and especially to elucidate details of the connected liquid structure, in terms of the normal modes of water molecules engaged in hydrogen bonding proved futile, for every hypothesis advanced was disproved by experiment. It was not until recently that the spectrum was analyzed in a manner that satisfied both theoretical description and experimental measurement. This was done by Green, Lacey, and Sceats (GLS), when they compared the liquid water spectrum with that for ice I.[11]

Ice I has an intense Raman mode at ~3100 $cm^{-1}$. This mode is a collective mode of ice. It represents an in-phase coupling of OH stretching motions; i.e., it is a measure of the strong

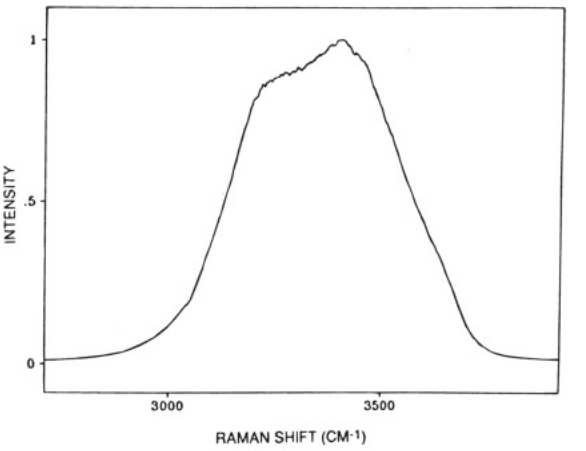


**Figure 4.** Linear Raman spectrum of water in the OH stretch region.

hydrogen bonding found in ice. GLS noted that the 3100-$cm^{-1}$ mode of ice shifted to higher frequency and broadened when the ice temperature was raised. They interpreted the shifting and broadening to be a result of the decrease in hydrogen bonding order which occurs when ice melts. GLS then monitored the liquid Raman spectrum, which contains two peaks, one at ~3250 $cm^{-1}$, another at ~3500 $cm^{-1}$, as a function of temperature. They noticed that as the temperature of water was decreased from 90 to −10 °C, the peaks shifted to lower frequencies (3200 and 3450 $cm^{-1}$, respectively), and the relative peak intensity ratio changed. The peak at 3500 $cm^{-1}$ lost intensity, while the peak at 3250 $cm^{-1}$ gained intensity. These observations lead GLS to suggest that in liquid water at 25 °C the peak at 3450 $cm^{-1}$ is due to a localized OH oscillator mode, i.e., chemically bonded O−H, while the peak at 3250 $cm^{-1}$ to is due to in-phase couplings of OH stretch motions, i.e., analogous to the collective OH mode seen in ice and representing hydrogen bonded O···H. The increase in the 3250-$cm^{-1}$ peak intensity with decrease in water temperature was interpreted to arise from an increase in hydrogen bonding which occurs upon cooling. GLS suggested that the 3250-$cm^{-1}$ liquid water peak would shift to ~3100 $cm^{-1}$ with supercooling. Hare and Sorensen have recently shown that this does indeed occur.[12]

The GLS interpretation shows that a measure of the extent of hydrogen bonding in liquid water can be obtained by comparing the integrated intensities of the 3250- and 3500-$cm^{-1}$ peaks. The peaks in the unpolarized liquid water Raman spectrum at 25 °C are not well resolved, but the separate contributions can be determined by comparing the isotropic and anisotropic Raman spectra generated when the signal polarization is analyzed.

## MDSRS Spectrum of Water in the OH Stretch Region

The MDSRS spectra we generate for pure water aerosols (those generated by using conditions that minimize acoustic contamination) at 25 °C show two, well-resolved peaks in the water OH stretch region. This is shown in Figure 5A. The peaks are centered at Raman shifts of 3245 and 3450 $cm^{-1}$, respectively. We assign these peaks to the collective and localized water modes, respectively. To verify our assignment, we have added a known hydrogen bond disrupter, LiCl, to the water used to generate our aerosols. Figure 5B shows the MDSRS spectrum generated from 1.4 M LiCl aerosols. The result shows that the MDSRS intensity at 3245 $cm^{-1}$ has decreased considerably, an observation which confirms our assignment. It is interesting to note how well resolved the collective and local mode peaks are, relative to that seen from linear Raman spectroscopy. This positive outcome is a result

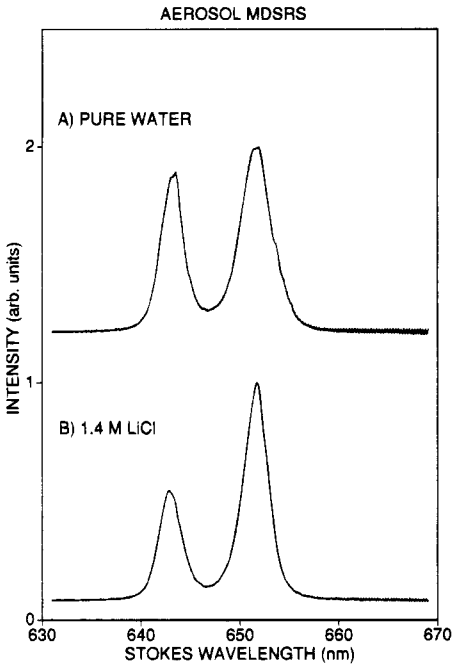


**Figure 5.** (A) MDSRS spectrum generated with a pure water aerosol. (B) MDSRS spectrum generated with a 1.4 M LiCl solution aerosol.

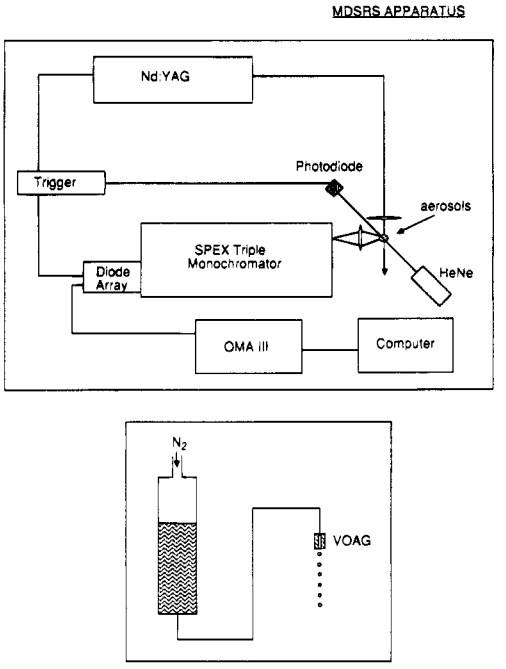


**Figure 6.** Schematic of the MDSRS apparatus.

of MDSRS's nonlinear nature. Signal intensity, $I_{MDSRS}$, is proportional to $\exp^{(N)}$, where $N$ is the number density.[6] Small changes in population are thus amplified in an MDSRS spectrum, and strongly overlapped peaks lift out from the background.

Our MDSRS spectra are equivalent to isotropic Raman spectra, for they have been generated with horizontally (p-) polarized light. To accurately determine relative populations in the collective and localized modes it is necessary to deconvolute the MDSRS spectrum. This can be done by comparing the integrated intensities of isotropic and anisotropic MDSRS Raman spectra (i.e., by measuring the parallel and perpendicular spectra generated by using an s-polarized incident laser) and using a deconvolution procedure developed by GLS.[11] These experiments will be done in the future. For now, we will only roughly quantify the relative hydrogen bonding by comparing the relative 3245- and 3450-$cm^{-1}$ peak intensities. We do this, however, to demonstrate that MDSRS is particularly suited for analyzing hydrogen bonding in aqueous systems and to show that aerosols created by using a VOAG suffer severe hydrogen bond disruption.

## Experimental Procedure

The procedure associated with aerosol MDSRS is extremely straightforward. A schematic of our apparatus is shown in Figure 6. A train of aerosols is generated by passing a pressurized solution of the species of interest through a vibrating orifice. The solution is pressurized by maintaining a constant $N_2$ pressure over a liquid reservoir. A 90° incident laser beam is focused (130-$\mu$m diameter) and directed to a position slightly to the right of the aerosol train axis (i.e., an edge illumination geometry). The driving conditions of the vibrating orifice are set to ensure that the spacing between the aerosols is sufficiently large such that only a single aerosol is illuminated by the laser at any one time, and a trigger system ensures that the incident beam targets the equatorial edge of a specified aerosol every time the laser is fired. The MDSRS signal is collected by a lens located at right angles to the input laser beam, imaged into a triple monochromator (0.6-nm resolution HWHM), dispersed,

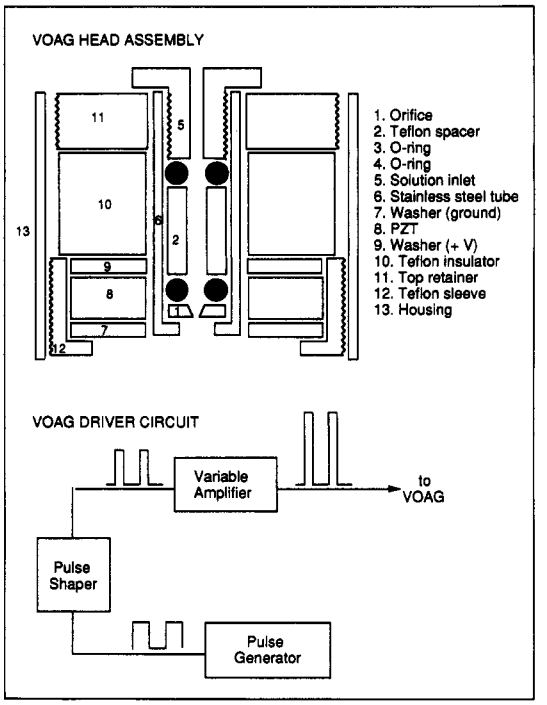


**Figure 7.** Vibrating orifice aerosol generator (VOAG) assembly and driving circuit.

and detected by a diode array (OMA III). The detector is cooled to −40 °C, and gated to be synchronous with the arrival of the laser pulse at the aerosol train. The detector gate width is set at 5 $\mu$s to ensure that all MDSRS is collected. This time gate corresponds to an aerosol cavity $Q$ factor of $3 \times 10^9$, a value which is three times larger than that predicted by theory.

Our vibrating orifice aerosol generator was fabricated by using the design of Worsnop et al.[13] A detailed schematic is shown in Figure 7. The VOAG tip basically consists of a 100-$\mu$m diameter Pt orifice (Structure Probe Inc. Model P6100) secured at the bottom of a lipped stainless steel tube (0.31-in. o.d.) with a buna O-ring and a Teflon spacer tube ($^1/_{16}$-in. i.d.). Liquid from the solution reservoir is fed into the VOAG through $^1/_{16}$-in. o.d. PTFE Teflon tubing. The VOAG tip is press fit into a

second assembly which contains the piezoceramic crystal (Channel Industry Corp. model C-5400, 0.688-in. o.d., 0.313 i.d., 0.250-in. thickness) used to induce mechanical vibrations. The piezoceramic is wired such that it vibrates in its "doughnut" mode. The entire VOAG assembly is screw-mounted on a Newport Model 705 Precision five-axis positioner, machined to accommodate the VOAG head.

Davidovits has noticed that the optimal conditions for generating a mechanically stable aerosol train occur when the piezoceramic is driven by a short-duration, square-wave, 40-V (peak-to-peak) pulse.[14] The electronic circuitry used to generate these pulses is given in Figure 7. The circuit basically consists of a high-precision frequency generator (Hewlett-Packard Model 3336C) which produces a square wave. The square wave is then fed through a Rutherford Model 816 pulse shaper. This latter instrument produces an adjustable-width square-wave pulse. We used a pulse width of 5 $\mu$s in the experiments. The square-wave pulse was then fed through a variable amplifier (University of Pittsburgh Electronics Shop) to boost the voltage. We found that a 30-V pulse produced the most stable aerosol train.

The size and spacing of aerosols created by a VOAG is determined by the volume flow rate of solution through the orifice and the vibrating frequency. The flow rates for liquid reservoir backing pressures of 20, 40, and 60 psi were measured as 0.115, 0.158, and 0.202 $cm^3\ s^{-1}$ and give aerosol train velocities of 1468, 2015, and 2572 cm $sec^{-1}$, respectively. To produce aerosols with equivalent diameters, the vibrating frequency was increased with the flow rate; vibrating frequencies of 35.4 $\pm$ 1.1, 51.3 $\pm$ 1.1, and 64.7 $\pm$ 1.1 kHz generated aerosols with diameters of 184, 181, and 181 $\mu$m at backing pressures of 20, 40, and 60 psi, respectively.

The size and velocity of the individual aerosols contained in the train was monitored by focusing a HeNe laser beam (85-$\mu$m diameter) at the aerosol train and monitoring the beam intensity depletion with a fast response photodiode (MDR500). The HeNe beam intersected the aerosol train 2.5 cm below the VOAG tip. The photodiode signal, which is used to trigger the Nd:YAG laser and diode array detector, was monitored by a Hewlett-Packard 54601A 100-MHz digital storage oscilloscope. The variation in aerosol diameter and spacing in the train, which is determined by monitoring the temporal characteristics of the photodiode signal, was less than the resolution of the oscilloscope, which corresponds to a variation of $<\pm 0.07\%$ in both aerosol diameter and spacing.

The water used in the experiments was obtained from a Barnstead NANOpure UV water filtration system. The resistivity of the water was measured at 18 M$\Omega$ cm. The water was transported directly to the VOAG liquid reservoir and additionally filtered through a set of decreasing pore size Barnstead disposable filter units (DQ, BQ, and AAQ, which have pore sizes of 25, 2, and 0.3 $\mu$m, respectively) located at the exit of the liquid reservoir.

The aerosols were expanded into room air (1 atm, 25 °C) that was saturated with respect to water vapor. Our VOAG apparatus is contained in a ~2 ft × 3 ft × 2.5 ft anodized aluminum/Plexiglas chamber. A filled pan of water was placed in the chamber to saturate the environment with water vapor. This procedure was followed to ensure that the freshly generated aerosols did not evaporate while they fell from the VOAG tip. Evaporation can induce temperature gradients at the aerosol surface and lower the MDSRS sensitivity.

The 532-nm laser beam intersects the aerosol train at a distance 7 cm below the VOAG tip, thus the aerosols generated at 20, 40, and 60 psi backing pressure are probed 4.76, 3.47, and 2.72 ms after they have exited the VOAG tip, respectively. The aerosols are illuminated with 2.5 mJ/pulse laser energy. This corresponds to an intensity of $3 \times 10^9$ W $cm^{-2}$ at the focal point. The intensity of light coupled into a green internal cavity mode is determined by the ratio of the laser linewidth to the green mode linewidth, i.e., $\phi = \Delta\nu_{laser}/\Delta\nu_{MDR}$, thus cavity modes with $Q = 1 \times 10^9$ range soak up only 0.01% of the incident intensity. Aerosol heating does not occur as a result, for not only is the local mode intensity low, but the water comprising the aerosol has negligible absorption, i.e., $\alpha < 0.0005$ $cm^{-1}$, as measured with a UV−vis spectrometer.

Incident laser intensity was purposefully kept low to prevent MDSRS signal saturation. We monitored the MDSRS water signals generated for incident pulse energies ranging from 0.5 to 8 mJ. The log ratio of the peak intensities at 3245 and 3450 $cm^{-1}$ was identical for incident intensities below 6 mJ/pulse. Intensities higher than this caused saturation, as evidenced by a decrease in 3450-$cm^{-1}$ intensity. The MDSRS signal entering the monochrometer was attenuated with neutral density filters with transmissivities of $T = 0.002-0.037$. The MDSRS signal from water is very intense because the concentration, 55.5 M, is large.

Individual MDSRS spectra were collected by coadding the signals generated from 30 individual laser shots. The results contained in ~30 individual spectra, collected under identical conditions, were averaged to obtain the data points presented below. Data was generated for three sets of experimental conditions. In one set of experiments, water from the Barnstead filtration unit was used immediately. This water contains solubilized $N_2$ and $O_2$ gas at equilibrium conditions that correspond to 25 °C and 1 atm pressure. In these experiments the data acquisition time was limited to 1.5 h to ensure that the water was not contaminated with $N_2$ gas which diffuses in from the top of the liquid reservoir. In the following we label this experimental condition as "equilibrium gas". In the second set of experiments, the water was exposed to reservoir $N_2$ pressures of 20, 40, and 60 psi overnight (15 h) to increase the amount of solubilized gas. We label these experimental conditions as "excess gas". In the third set of experiments, the gas-pressurized liquid reservoir was replaced with a large-volume Hamilton syringe, and the water in the syringe was first boiled and then vacuum pumped for 2 h to remove all gas. This experimental condition is labeled as "no gas".

## Results

The MDSRS spectra of water aerosols generated for the above-listed experimental conditions are shown in Figure 8. The spectra located on the left side of this figure were generated with the incident laser coming in at almost grazing incidence with the aerosol equatorial edge. This particular illumination geometry causes red modes located fairly deep in the aerosol, in a region ~5.5 $\mu$m below the surface, to be excited. The spectra therefore correspond to the condition of the bulk liquid water comprising the aerosol and are labeled as such. The spectra on the right of Figure 8 correspond to conditions where MDRs located closer to the surface, ~1 $\mu$m deep, were excited. This was accomplished by translating the incident laser beam away from its initial grazing incidence equatorial edge illumination geometry. We label this condition as edge illumination. The spectra are plotted as a function of time after the aerosols have left the VOAG tip. The times are listed in the center portion of Figure 8, along with the condition of the liquid passed through the vibrating orifice.

The spectra in Figure 8 show a very interesting trend. The results show that the intensity of the 3245-$cm^{-1}$ peak, which

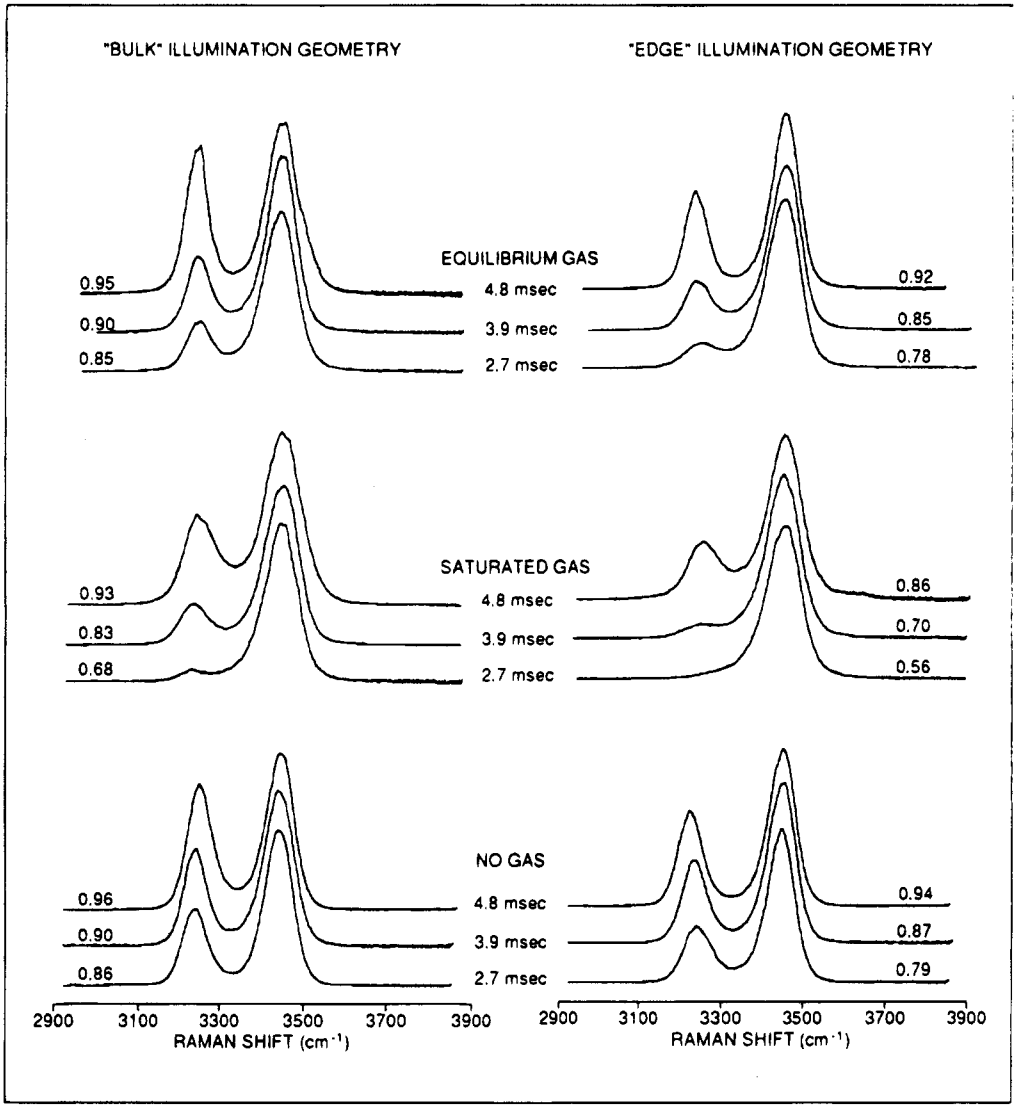


**Figure 8.** MDSRS spectra of aerosols generated by passing water containing equilibrium, saturated, and no solubilized $N_2$ gas through a vibrating orifice aerosol generator. Spectra on the left correspond to illumination of material located ~3.5 $\mu$m below the aerosol surface. Spectra on the right correspond to a region ~1 $\mu$m from the surface. The times listed in the central portion of the figure correspond to the aerosol age.

corresponds to hydrogen-bonded OH, decreases rather dramatically with decreasing aerosol age. We define here an approximate quantitative measure of the hydrogen bonding in the system. In Figure 4 we show a linear Raman spectrum of water at 25 °C. The intensity at a Raman shift of 3245 $cm^{-1}$ is slightly smaller than the intensity at a Raman shift of 3450 $cm^{-1}$. The ratio, $I_{3245}/I_{3450}$, is 0.95 ± 0.01. We define this ratio as the ratio which represents water in an undisrupted state. MDSRS signal scales exponentially with linear Raman intensity, i.e., $I_{MDSRS} \alpha \exp^{N(d\sigma/d\Omega)}$, where $N$ is the concentration (molecules $cm^{-3}$) and $(d\sigma/d\Omega)$ is the Raman cross section ($cm^2$ $molecule^{-1}$ $sr^{-1}$).[6] Thus the log ratio of the measured MDSRS peak intensity at 3245 and 3450 $cm^{-1}$, ln $I_{3245}$/ln $I_{3450}$, is a measure of the hydrogen bonding in the system. We define this as the hydrogen bond ratio, HBR. The HBRs, determined by averaging 30 data sets collected for each of the above-listed experimental conditions, are listed to the left and the right of the bulk and the edge illumination spectra, respectively.

The HBRs in Figure 8 show several distinctive trends. All data sets show that the HBR value at the earliest time delay is much smaller than the 0.95 ± 0.01 equilibrium value. These results show that the VOAG initially creates aerosols that are structurally impaired. The HBR values all increase with increasing time out of the VOAG tip, suggesting that an equilibrium condition is slowly being achieved. We note, however, that under certain conditions equilibrium has not been achieved, even at time delays of 4.7 ms.

A comparison of the spectra generated for both bulk and edge illumination geometries shows that the hydrogen bond disruption is more pronounced at the aerosol edge. For example, the HBRs for bulk water at equilibrium gas concentration are 0.85 ± 0.03, 0.90 ± 0.03, and 0.95 ± 0.02 at time delays of 2.7, 3.9, and 4.8 ms, while those measured in the region closer to the surface are 0.79 ± 0.03, 0.85 ± 0.03, and 0.92 ± 0.03, respectively. We note here that it is highly improbable that we are seeing outer interface structural changes that are predicted to occur by molecular dynamics simulations and seen recently by sum frequency experiments.[15,16] It is now established that interfacial water is structurally different from bulk, the principal difference being that the surface water molecules are not as well hydrogen bonded as the bulk water molecules. Molecular dynamics simulations show that the transition from 3-D to 2-D hydrogen bonding occurs over a 20-Å region.[15] Our MDSRS has a minimum spatial resolution of ~4 nm, due to the diffraction limitation, and we are probing ~1 $\mu$m from the outer surface. The change in hydrogen-bonding character of the liquid we observe most likely reflects an increase in the effect which causes the hydrogen bond disruption, at the surface.

Hydrogen bonding becomes even more perturbed when a solution saturated with gas is flowed through the vibrating orifice. The HBRs measured for bulk and edge illumination geometries are 0.68 ± 0.03, 0.83 ± 0.03, 0.93 ± 0.02, and 0.56 ± 0.03, 0.70 ± 0.03, and 0.86 ± 0.03, at time delays of 2.7, 3.9, and 4.8 ms, respectively. The decrease in the HBR upon addition of $N_2$, which does not hydrogen bond with water, is expected. The spectra show that the hydrogen bond disruption induced by the added gas is more severe at the aerosol surface, as compared with the bulk. This suggests that there may be a gas concentration gradient, with the maximum at the surface, set up in the VOAG. We note that the VOAG is a sonicator in disguise. Gas molecules will preferentially congregate at the VOAG inner wall surface dislocations. The flow through the orifice is laminar, thus the internal gas gradient will reflect itself in the aerosols.

The VOAG-as-sonicator view is confirmed by the observation that small gas bubbles form on the surface of aerosols generated with a saturated gas solution. When the optically excited aerosols are viewed with a microscope objective and a green filter, small hollow circles of red intensity maxima are seen superposed on the regular MDSRS intensity distribution. Rayleigh scattering from these bubbles could reduce the HBR, since the scattering cross section is larger at 643 nm (the Stokes wavelength of the 3245-$cm^{-1}$ peak) than at 651.6 nm (the Stokes wavelength of the 3450-$cm^{-1}$ peak), but this mechanism can account for a decrease of only 5% in the HBR. The Campillo group has also noticed that bubbles form in aerosols generated with a VOAG and has used imaging photography to verify their presence.[17]

Complete removal of gas from the VOAG solution improves the aerosol structure, but there are still structural defects imposed by the vibrating orifice. The HBR ratios measured in the bulk at 2.7, 3.9, and 4.8 ms are 0.86 ± 0.03, 0.90 ± 0.03, and 0.96 ± 0.03. These values are somewhat larger than the values measured for bulk solution at equilibrium gas concentration, but it is difficult to decide if there is any real change, for the differences between the "no gas" and "equilibrium gas" values are within experimental error. The results for edge iluumination still show that some perturbation is present, for the interface HBRs are smaller than those seen for the bulk and are 0.79 ± 0.03, 0.87 ± 0.03, and 0.94 ± 0.03 at the time delays just listed.

We do not see any appreciable shifting of peak position in the collective or local OH modes with change in experimental conditions. This is a consequence of the fact that our monochromator does not have sufficient resolution to distinguish any expected changes. Green, Lacey, and Sceats have shown that both the collective and local OH frequencies shift upward by only 50 $cm^{-1}$ over a temperature change of 100 °C (i.e., in the −10 to 90 °C range).[11] This shift is within our monochromator resolution.

## Discussion

The MDSRS results show that a long-lived disturbance, which manifests itself by disrupting the water hydrogen bonding, is present in aerosols generated with a vibrating orifice. The results also show that the disturbance is more pronounced at the aerosol surface. The disturbance is unusual in that the relaxation of the hydrogen bonding back to equilibrium cannot be characterized by a single decay constant. For example, Figure 9 plots the logarithm of the HBR ratio at equilibrium minus that measured as a function of time for all six experimental conditions. None of the plots are linear, all are quadratic in character, and an inspection of the data shows that equilibrium has been achieved only after 5 ms in the "no gas" and

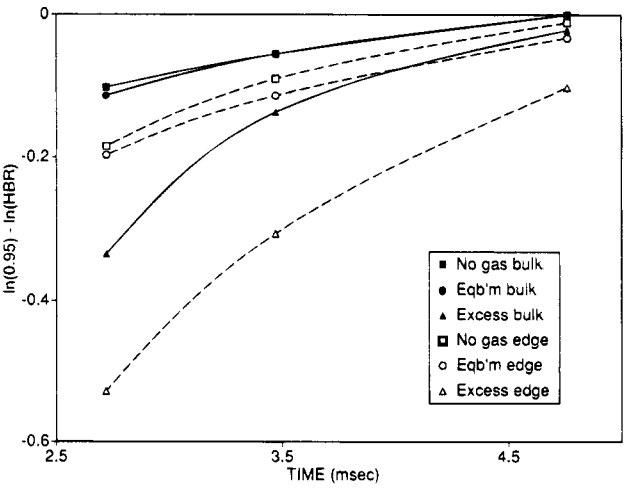


**Figure 9.** Time-dependent behavior of the hydrogen bond ratios measured for the "bulk" and "edge" aerosol liquid. Solid lines and symbols correspond to the "bulk", hollow symbols and dashed lines are for "edge".

"equilibrium gas" bulk samples. The "excess gas" bulk sample and all edge samples have not come to equilibrium.

The root cause of the hydrogen bond disruption is not known, but we can eliminate several possible sources. Hydrogen bonding is known to be strongly affected by temperature, pressure, organic and inorganic impurities, and the presence of an electric field. As we show below, it is unlikely that the disruption is caused by thermal, impurity, or electric field effects. We think that the disruption is caused by a pressure effect. But before we present our arguments, we first outline some further details of MDSRS to show that the observed hydrogen bond disruption is not an artifact of nonlinear signal generation.

We have previously shown that MDSRS signal gain is given by[6]

$$I_{\mathrm{MDSRS}} = \exp[\phi I_o A\, N(\mathrm{d}\sigma/\mathrm{d}\Omega)\, Q_{\mathrm{red,real}}{}^2] \qquad (4)$$

where $I_o$ is the incident intensity (W $cm^{-2}$), $A = 8\pi^2 c^3 m_{\mathrm{green}}/h\omega_{\mathrm{green}}\omega_{\mathrm{red}}{}^4 m_{\mathrm{red}}{}^3$, $N$ is the number density (molecule $cm^{-3}$), and $(\mathrm{d}\sigma/\mathrm{d}\Omega)$ is the Raman cross section ($cm^2$ molecule$^{-1}$ $sr^{-1}$). $\phi$ is the fraction of input light coupled into the output red MDR, $\phi = (Q_{\mathrm{laser}}/Q_{\mathrm{calc,green}})(Q_{\mathrm{calc,green}}/Q_{\mathrm{calc,red}})$, where $Q_{\mathrm{calc}}$ is that determined by Mie scattering theory. The aerosols used in our experiment (182−184-$\mu$m diameter) have $n = 870-1170$ and $l = 1-50$, and Mie calculated $Q$ values which range from $10^{12}$ to $10^{162}$. The calculated $Q$ values are unrealistic because theory does not account for minute variations in the refractive index caused by molecular reorientation. We have previously shown that a simple modification can correct the theory, i.e., $1/Q_{\mathrm{calc}} = 1/Q_{\mathrm{Mie}} + 1/Q_{\mathrm{mol}}$, where $Q_{\mathrm{mol}} = \omega/\Gamma$, and $\Gamma$ is the molecular reorientation time. If $\Gamma$ is unknown it can be estimated by noting the time it takes a sound wave to travel the circumference of an MDR, i.e., $1/\Gamma \sim 2\pi r_{\mathrm{MDR}}/v_{\mathrm{sound}}$. Our particular aerosols' theoretical $Q$ values are thus limited to being $1 \times 10^9$, and as a result, $\phi = 10^{-4}$, since $Q_{\mathrm{laser}} = 10^5$ in our experiment. What this means is that for the aerosols used in our experiment, all MDRs (associated with water aerosols which have diameters between 180 and 186 $\mu$m) have identical $Q_{\mathrm{calc}}$, identical $\phi$, and therefore identical input intensity. Provided that $Q_{\mathrm{red,real}}$ is independent of MDR identity, then $I_{\mathrm{MDSRS}}$ will simply reflect the number density of species being probed in the aerosol region physically accessed by the MDR. We note here that the Mie calculations are done for perfect spheres, while in the experiments the aerosols assume an oblate shape as they flow from

the orifice tip. The deviation from perfect sphericity shifts the MDR spectra profile (by $<1$ cm$^{-1}$), but as shown by Chang et al. it does not influence the magnitude of $Q$.[18]

When considering the extent of MDR participation in a specific optical signal generation event, the $Q$ value must be modified to account for the fact that competition from other optical processes will occur. For stimulated Raman scattering, the MDR $Q$ value is modified by

$$1/Q_{\text{red,real}} = 1/Q_{\text{calc,red}} + 1/Q_{\text{a}} = 1/Q_{\text{Rayleigh}} + 1/Q_{\text{ref}} \quad (5)$$

where $Q_{\text{a}}$ and $Q_{\text{Rayleigh}}$ reflect the degree of competition by absorption and Rayleigh scattering off foreign particulate matter or material occlusions. $Q_{\text{a}} = m/2k$, where $k$ is the imaginary part of the refractive index, $k = \alpha\lambda/4\pi$. $Q_{\text{Rayleigh}} = 2\pi m/\lambda\sigma_{\text{Rayleigh}}N_{\text{scat}}$, where $\sigma_{\text{Rayleigh}} = 32/27(m - 1)^2(2\pi r_{\text{scat}}/\lambda)^4\pi r_{\text{scat}}^2$, and $N_{\text{scat}}$ is the number density of scatterers in cm$^{-3}$. $Q_{\text{ref}}$ accounts for MDR degradation which arises from gradients in the refractive index. Optical dispersion is a typical example, i.e., $Q_{\text{ref}} = m/\Delta m$, where $\Delta m$ is the refractive index change which spans the MDR linewidth. Second- and higher- order optical effects, such as self-phase modulation and focusing, and the optical-field-induced refractive index change can be ignored in our experiment as the local MDR intensity is well below the threshold (i.e., $I_{\text{MDR}} = I_0\phi = 2.4 \times 10^9$ W cm$^{-2} \times 10^{-4} = 0.2$ MW cm$^{-2}$). If it is assumed that absorbers and scatterers are uniformly distributed throughout the aerosol sample, and that the refractive index and optical dispersion is likewise uniform, then all MDRs will have identical $Q_{\text{real,red}}$ values, and the MDSRS spectra will be free of artifacts imposed by the nonlinear signal generation process. If this assumption is invalid, then the spectra must undergo a more detailed analysis. We do this now.

An HBR ratio $<0.95$ can be obtained only if (a) the number density of the hydrogen-bonded water is less than the equilibrium value or (b) $Q_{643} < Q_{653}$. For the latter to occur, the spatial overlap of the 643-nm mode (corresponding to a Stokes shift of 3245 cm$^{-1}$) would have to be less than that of the 652-nm mode (3400-cm$^{-1}$ Stokes shift). As stated earlier, red modes couple with green modes when their $n_m$ azimuthal mode numbers match. There does not have to be a match in angular mode number, $n$, but for appreciable spatial overlap to occur, the $r_{\text{MDR}}$ must be identical, a result which necessitates that the modes' $l$ values be identical. Since $r_{\text{MDR}} \sim (n + 1/2)\lambda/2\pi m$, the $n$ associated with the 643-nm mode is larger than that of the 652-nm mode. A simple geometric calculation shows that the overlap in the angular dimension is given by $(2n_{\text{red}} + 1)/(2n_{\text{green}} + 1)$; hence, the overlap associated with the 643-nm mode is larger (albeit slight) than that associated with the 652-nm mode. The means that $Q_{643} > Q_{652}$, and so the observed hydrogen bond disruption does not stem from an artifact of nonlinear signal generation. In fact our MDSRS spectra *underestimate* the extent of hydrogen bond disruption.

We have noticed that our absolute signal intensity decreases when we image the edge region of the aerosol. While a slight intensity decrease is expected from theoretical considerations,[7,9] the observed decrease is larger than predicted. This $Q$ factor degradation can stem from either impurities congregating at the surface or from a refractive index gradient. We do not think it is the former for we have carefully analyzed the product aerosol liquid using UV/vis and IR spectroscopy and have been unable to detect any contaminants.

We suspect that the extra $Q$ factor degradation stems from a refractive index gradient. But since this cannot be a result of the presence of impurities, or gas bubble Rayleigh scatterers in the "no gas" case, then clearly it must come from a molecular structure change. This conclusion is corroborated by our observation of hydrogen bond disruption. We can think of only three other phenomena which can explain the observed hydrogen bond disruption. These are an electric field effect, a thermal effect, and a pressure effect.

The vibrating orifice creates aerosols that have a permanent surface charge. The aerosols associated with our apparatus have a total negative charge of $\sim 8 \times 10^{-12}$ C, but this value does decrease with a decrease in the voltage applied to the VOAG piezoceramic. We determined the charge magnitude by noting the distance the aerosol train is deflected when a negatively charged plate is brought up to the stream at a distance 15 cm from the orifice tip. The surface charge is rather hefty, and so the hydrogen bond disruption observed in our aerosols may stem from the alignment of the water molecules by the electric field at the surface. This effect could explain the increase in hydrogen bond disruption seen at the aerosol surface; however, the voltage applied to the piezoceramic was identical for all six data sets generated, and we would expect to see no difference in hydrogen bond disruption as a function of aerosol age since the charge is permanent.

Hydrogen bonding is strongly influenced by temperature. There are two thermal effects associated with our experiment; aerosol heating by the incident laser or aerosol cooling by evaporation. The local change in temperature in the region encompassed by an MDR induced by laser heating can be estimated by using the formula given by Lin et al.:[19] $\Delta T_{\text{MDR}} = \alpha\Delta t I_{\text{MDR}}\nu_{\text{Raman}}/(\nu_{\text{excite}}\varrho c)$, where $\alpha$ is the Lambert absorption coefficient (0.0005 cm$^{-1}$ for our aerosols), $\Delta t$ is the laser pulse width (6 ns), $I_{\text{MDR}} = 0.2$ MW cm$^{-2}$ (see above), $\nu_{\text{Raman}} = 3450$ cm$^{-1}$, $\nu_{\text{excite}} = 18\,797$ cm$^{-1}$, $\varrho = 1.006$ g cm$^{-3}$, and $c$ is the specific heat (1 cal g$^{-1}$ °C$^{-1}$). In our experiment $\Delta T_{\text{MDR}} = 1 \times 10^{-7}$ °C. This temperature change is too small to induce structural disruption. In addition, if laser heating were occurring, it would be independent aerosol age. Our results contraindicate this.

A temperature gradient could be set up by evaporative cooling. Our experiments were designed to minimize this effect for we expanded the aerosols into room temperature air that was saturated with water vapor. If evaporation were occurring we would expect to see an increase in the HBR at the aerosol surface, for hydrogen bonding increases with decreasing temperature. We see the opposite. We note, however, that a slight temperature gradient could induce capillary wave formation at the aerosol surface, and these waves can disrupt the hydrogen bonding. However, the depth of these waves is expected to be 10 Å at the most, and not the $\sim 1$ $\mu$m we see.

The only other phenomenon known to cause hydrogen bond disruption is pressure, and it is well established that the HBR decreases with increasing pressure.[20] There are two sources of pressure disturbance in our experiments: (a) pressure changes induced by shape distortions of the aerosols and (b) pressure waves associated with an acoustic disturbance that is trapped inside the aerosols.

It is highly unlikely that the hydrogen bond disruption observed stems from minute pressure fluctuations induced in the aerosols while they undergo a series of shape distortions as they evolve from the orifice tip. When an aerosol leaves the orifice and starts its free fall, it is longer in the vertical than in the horizontal direction. Surface tension causes the drop to pull back into a spherical form, but there is some overcompensation. The end result is that the aerosol undergoes a series of shape oscillations. The frequency of oscillation is determined by $\omega^2 = (2/\pi^2)\gamma/a^3\varrho$, where $\gamma$ is the surface tension, $a$ is the aerosol radius, and $\varrho$ is the density.[21] The frequency of our aerosols'

shape distortion is $\sim 4.4 \times 10^3$ Hz. Shape oscillations are rapidly damped. As shown by Lamb,[22] the damping constant is $\tau = a^2/5\nu$, where $\nu$ is the kinematic viscosity ($\nu = \eta/\varrho$ where $\eta$ is the viscosity). Our aerosols have $\tau = 1.85$ ms. These shape oscillations will induce small pressure fluctuations that are equivalent to fluctuations in capillary pressure. As given by Bikerman, $\Delta P_c = 4\gamma/\lambda$, where $\lambda = (2\pi\gamma/\omega^2\varrho)^{1/3}$.[21] The shape distortions induce a maximum change in pressure of only $10^{-2}$ atm. Thus they cannot be the root cause of the severe hydrogen bond disruption seen in our experiments.

The trends in our water MDSRS data, and our experimental observation of bubble formation, lead us to suggest that a pressure disturbance which is created by a trapped acoustic wave is responsible for the hydrogen bond disruption seen in aerosols produced with a vibrating orifice aerosol generator. Previous Raman spectroscopic studies show that the degree of hydrogen bonding in liquid water decreases with increasing pressure and/or temperature. For example, Walrafen et al. have shown that all hydrogen bonding in liquid water is destroyed at 3250 atm and 200 K.[20] Acoustic waves generate microscopic sized areas of high local pressure and temperature. For example, the collapse pressure and temperature associated with a low intensity (0.1 W cm$^{-2}$) acoustic source are 4000 atm and 200 °C.[23] These temperatures and pressures are large enough to break water molecule chemical bonds, as evidenced by the observation that water sonication creates H• and OH• radicals.[23] It is therefore not unrealistic to assume that in the presence of an acoustic wave the relatively weak hydrogen bonds will also dissociate. As we noted earlier, the VOAG apparatus is simply a small sonicator in disguise, and the frequencies it is operated at, 20–70 kHz, are typical of the frequencies used in sonic-enhanced chemistry experiments, foaming and emulsion generators, and sonic cleaning apparatus. Our observation that bubbles form on the surface of our aerosols reinforces the idea that an acoustic disturbance is present, for sonication is commonly used to degas liquids.

The observed hydrogen bond disruption survives in our aerosols several milliseconds after they exit the orifice tip. This result suggests that a pressure disturbance must be trapped inside the newly formed aerosols. The observed hydrogen bond disruption cannot be the result of a single transient pulse. The structural relaxation time of water is extremely short, $\sim 10^{-11}$–$10^{-12}$ s, thus the liquid comprising the aerosol would have relaxed back to its equilibrium configuration long before we bring in our laser probe. The acoustic wave that forces the aerosol from the VOAG tip can, however, be trapped inside the aerosol, for reflection at the water–air interface is very efficient (alternatively, transmission is very inefficient). Pressure disturbances can result from the continued reverberation of this acoustic wave.

The power reflection, $\alpha_r$, coefficient at the water–air interface is a complicated function of the velocity of sound and density in the two media and the angle of incidence:[24]

$$\alpha_r = [(\varrho_2 c_2 \cos\theta_i - \varrho_1 c_1 \cos\theta_t)/(\varrho_2 c_2 \cos\theta_i + \varrho_1 c_1 \cos\theta_t)]^2 \quad (6)$$

where the subscripts 1 and 2 denote the medium from and into which the acoustic wave is traveling, $\varrho$ is the density, $c$ is the sound velocity, $\theta_i$ is the incident angle, and $\theta_t$ the transmission angle, given by $\sin\theta_t = c_2 \sin\theta_i/c_1$. For normal incidence, $\alpha_r = 0.9988$ at the water–dry air interface.[24] At angles of incidence away from normal, $\alpha_r$ increases to 1.0. Acoustic attenuation by water is minimial at the frequencies used in our experiments, $\alpha \sim f^2(18 \times 10^{-17})$ cm$^{-1}$,[24] thus attenuation of the acoustic wave launched in an aerosol at its nascence will arise principally from transmission losses that will occur at each reflection, i.e., $I/I_0 = \exp(-\alpha_r N)$, where $N$ is the number of reflections. Obviously waves incident normal to the surface will attenuate more rapidly than those incident at oblique angles.

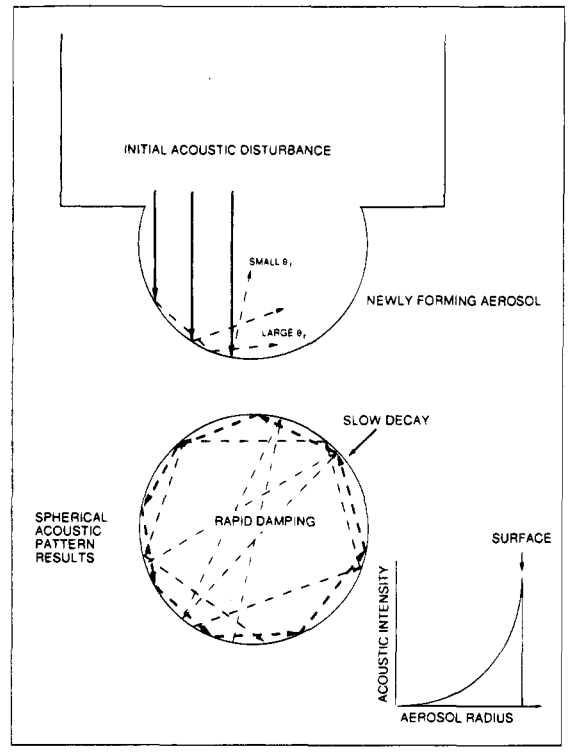


**Figure 10.** A spherical acoustic wave pattern is created when an initial acoustic disturbance becomes trapped in an aerosol while it is being generated.

If an acoustic wave is launched into the aerosol while it is being formed, a spherical acoustic wave pattern can be set up. Figure 10 illustrates this. As the incident acoustic wave travels down through the aerosol body, successive portions of its initial intensity will be reflected off, due to the fact that the aerosol surface is curved. A new subset of spherical waves is thus generated. The temporal character of this new subset of waves will be rather complicated, for each new wave generated will have a unique $\theta_i = \theta_r$ and therefore $\alpha_r$. Notice that waves with small $\theta_r$ attenuate more rapidly than waves with large $\theta_r$, and so acoustic waves mirrored directly back into the aerosol interior will decay rapidly, while those waves that just skim around the surface will decay very slowly. The net result is that an acoustic intensity gradient is set up, with the maximum at the aerosol surface and the minimum at the aerosol center. This intensity gradient can explain our observed increase in hydrogen bond disruption at the aerosol surface. We note that the decay in acoustic intensity cannot be characterized by a single $\tau$, for waves located closer to the aerosol surface will damp more slowly than those located in the interior. Our MDSRS data (see Figure 9) also reflect this complicated temporal trend.

## Conclusions

MDSRS is a rather unique spectroscopic technique that is especially suited for detailing the reactive properties of atmospheric aerosol interfaces. Previous studies in our laboratory have shown that MDSRS can be used to analytically monitor the chemical composition at the aerosol interface.[6] The experiments outlined here show that MDSRS can be used to determine the type and extent of bonding present. When put together, these observations demonstrate that MDSRS can be used to

obtain detailed molecular pictures of the aerosol interface. These molecular pictures will, of course, enable a more solid understanding of atmospheric aerosol heterogeneous processing potential to be developed.

The ability to use MDSRS to determine the type and extent of bonding present at the interface is important. But the experiments outlined here also demonstrate something more exciting. We have shown that MDSRS is highly location specific and that by simply changing the illumination geometry parameters, it is possible to walk from the bulk through the interface and take molecular "snapshots" along the way. It has been suspected for some time now that compositional and structural changes occur upon traversal from the bulk to the liquid surface. Indeed recent SHG studies of the air−water interface show that the chemical composition of the outer monolayer differs quite markedly from that in the bulk.[25] MDSRS can be used to scrutinize the chemical changes in great detail, and the results obtained will complement the information obtained from SHG and SFG studies. The spatial resolution afforded by MDSRS is limited by diffraction to being ~4 nm. This resolution excludes us from being able to take "snapshots" molecular layer by molecular layers. But a comparison of spectra obtained at different locations will certainly allow a qualitative description of the structural change at the interface to be developed.

The experiments outlined here show that aerosols generated with a vibrating orifice are structurally impaired, i.e., the water comprising the aerosol is in a state of severe hydrogen bond disruption. An analysis of our data suggests that the hydrogen bond disruption is caused by pressure disturbances induced by spherical acoustic waves trapped in a region close to the aerosol surface. Our evidence is indirect, but this explanation is the one that best fits our measured data. In future experiments we will be examining MDSRS signals from water molecule acoustic modes. Results from these experiments will enable us to confirm that an acoustic wave is the source of the observed hydrogen bond disruption.

The experimental results presented here clearly demonstrate that the surfaces of aerosols created by a VOAG are not at equilibrium, at least for the first 5 ms of their lives. While the nonequilibrium condition gives the aerosol surfaces unique physical and chemical properties, they do not, however, mimic those found in the natural atmosphere. We therefore recommend that extreme caution be used when interpreting the results of atmospheric modeling calculations that have used mass accommodation coefficients determined by laboratory experiments that have used VOAG generated aerosol surfaces. Our studies emphasize that it is extremely important that the structure of surfaces used in laboratory studies of heterogeneous atmospheric systems be well characterized. Simple monitoring of the depletion of gas-phase species is not sufficient, reactant aerosol surfaces need to be well parametrized to ensure that the heterogeneous system represents that found in the atmosphere.

**Acknowledgment.** This research is supported by the Office of Energy Science, Department of Energy, Division of Atmospheric and Climate Research, DE-FG02-91ER61204, and the National Science Foundation, Division of Atmospheric Chemistry, ATM-9118989. We thank the Asher group for generating the linear water Raman spectrum given in Figure 3.

## References and Notes

(1) World Meteorological Organization (WMO). *Scientific Assessment of Ozone Depletion: 1991*; Global Ozone Research and Monitoring Project, Rep. 25.; Washington, DC, 1991.

(2) For a review of all work done on liquid surfaces, see: Kolb, C. E.; Worsnop, D. R.; Zahniser, M. S.; Davidovits, P.; Hanson, D. R.; Ravishankara, A. R.; Keyser, L. F.; Leu, M.-T.; Williams, L. R.; Molina, M. J.; Tolbert, M. A. In *Current Problems and Progress in Atmospheric Chemistry*, Ng, C.-Y., Ed; Adv. Phys. Chem., 1994.

(3) Qian, S.-X.; Snow, J. B.; Tzeng, H.-M.; Chang, R. K. *Science* **1986**, *231*, 486.

(4) Lin, H.-B.; Huston, A. L.; Eversole, J. D.; Campillo, A. J. *Opt. Soc. Am.* **1990**, *B7*, 2079.

(5) Pinnick, R. G.; Fernandez, G. L.; Xie, J.-G.; Ruekgauer, T.; Gu, J.; Armstrong, R. L. *J. Opt. Soc. Am.* **1992**, *B9*, 865.

(6) (a) Zhang, J.-X.; Aker, P. M. *J. Chem. Phys.* **1993**, *99*, 9366. (b) Zhang, J.-X., Aiello, D., Aker, P. M. *J. Geophys. Res.*, in press.

(7) (a) Hill, S. C.; Benner, R. E. In *Optical Effects Associated with Small Particles*; World Scientific Publishing Co.: Singapore, 1988; Chapter 1. (b) Esam, E.; Khaled, M.; Hill, S. C.; Barber, P. W.; Chowdhury, D. Q. *Appl. Opt.* **1992**, *9*, 1166.

(8) Lam, C. C.; Leung, P. T.; Young, K. *J. Opt. Soc. Am.* **1992**, *B9*, 1585.

(9) Alexander, D. R.; Schaub, S. A.; Zhang, J.; Poulain, D. E.; Barton, J. P. *Opt. Lett.* **1989**, *14*, 548.

(10) Van de Hulst, H. C. In *Light Scattering by Small Particles*; Dover Publications Inc.: New York, 1957.

(11) (a) Green, J. L.; Lacey, A. R.; Sceats, M. G. *Chem. Phys. Lett.* **1986**, *130*, 67. (b) Green, J. L.; Lacey, A. R.; Sceats, M. G. *J. Phys. Chem.* **1986**, *90*, 3958. (c) Green, J. L.; Lacey, A. R.; Sceats, M. G.; Henderson, S. J.; Speedy, R. J. *J. Phys. Chem.* **1987**, *91*, 1684. (d) Green, J. L.; Lacey, A. R.; Sceats, M. G. *J. Chem. Phys.* **1987**, *86*, 1841. (e) Green, J. L.; Sceats, M. G.; Lacey, A. R. *J. Chem. Phys.* **1987**, *87*, 3603.

(12) (a) Hare, D. E.; Sorensen, C. M. *J. Chem. Phys.* **1990**, *93*, 25. (b) Hare, D. E.; Sorensen, C. M. *J. Chem. Phys.* **1990**, *93*, 6954. (c) Hare, D. E.; Sorensen, C. M. *J. Chem. Phys.* **1992**, *96*, 13. (d) Hare, D. E.; Sorensen, C. M. *Chem. Phys. Lett.* **1992**, *90*, 605.

(13) Washington, G. N., private communication, 3/2/92.

(14) Davidovits, P., private communication, 2/29/92.

(15) (a) Stillinger, F. H.; Ben-Naim, A. *J. Chem. Phys.* **1967**, *47*, 4431. (b) Townsend, R. M.; Gryko, J.; Rice, S. A. *J. Chem. Phys.* **1985**, *82*, 4391. (c) Wilson, M. A.; Pohorille, A.; Pratt, L. R. *J. Phys. Chem.* **1987**, *91*, 4873. (d) Matsumoto, M.; Kataoka, Y. *J. Chem. Phys.* **1988**, *88*, 3233. (e) Townsend, R. M.; Rice, S. A. *J. Chem. Phys.* **1991**, *94*, 2207. (f) Lie, G. C.; Grigoras, S.; Dang, L. X.; Yang, D.-Y.; McLean, A. D. *J. Chem. Phys.* **1993**, *99*, 3933.

(16) Du, Q.; Superfine, R.; Freysz, E.; Shen, Y. R. *Phys. Rev. Lett.* **1993**, *70*, 2313.

(17) Campillo, A. J., private communication, 12/20/93.

(18) Tzeng, H.-M.; Long, M. B.; Chang, R. K.; Barber, P. W. *Opt. Lett.* **1985**, *10*, 209.

(19) Lin, H.-B.; Eversole, J. D.; Campillo, A. J. *Opt. Lett.* **1992**, *17*, 828.

(20) Walrafen, G. E.; Hokmabadi, M. S.; Wang, W.-H.; Piermarini, G. J. *J. Phys. Chem.* **1988**, *92*, 4540.

(21) Bikerman, J. J. In *Physical Surfaces*; Academic Press: New York, 1970.

(22) Lamb, H. In *Hydrodynamics*; Dover Publications: New York, 1945.

(23) Mason, T. J. In *Sonochemistry*; Mason, T. J.; Ed.; Royal Society of Chemistry: Cambridge, 1990.

(24) Kinsler, L. E.; Frey, A. R. In *Fundamentals of Acoustics*; John Wiley and Sons: New York, 1962.

(25) (a) Eisenthal, K. B. *Annu. Rev. Phys. Chem.* **1992**, *43*, 627. (b) Eisenthal, K. B. *Acc. Chem. Res.* **1993**, *26*, 636.

JP9407482